Proceedings of the International Symposium of Mechanism and Machine Science, 2017
AzCIFToMM – Azerbaijan Technical University
11-14 September 2017, Baku, Azerbaijan

Experimental Verification of Quasi-Static Equilibrium Analysis of a Haptic Device

Ibrahimcan GÖRGÜLÜ[1], Omar W. MAAROOF[1], Barış Taner[1], Mehmet İsmet Can DEDE[1], Marco CECCARELLI[2],

[1]Izmir Institute of Technology
IzTech Robotics Laboratory, Gülbahçe Mah., Urla, Izmir, Turkey
E-mail: candede@iyte.edu.tr
[2] University of Cassino and South Latium,
LARM Laboratory of Robotics and Mechatronics, Cassino, Italy
E-mail: ceccarelli@unicas.it

Abstract

HIPHAD v1.0 is a kinesthetic haptic device which was designed and manufactured in IzTech Robotics Laboratory. In this work, the quasi-static equilibrium analysis is carried out by including the gravitational effects. The calculations are verified through an experimental procedure and the results are presented to characterize the device performance

Keywords: R-CUBE, HIPHAD v1.0, Haptic Device, Quasi-Static Equilibrium Analysis, Parallel Mechanism.

1. Introduction

Kinesthetic haptic devices target at stimulating the human sensory systems responsible for acquiring the sense of location/configuration, motion, force and compliance. These sensory capabilities are generally located at the muscles, tendons and joints. In order to cope with the required stimulation activities, kinesthetic devices are designed to cover the workspace of the targeted body part and their force display capabilities are designated to be in the range of the human capabilities.

A variety of solutions exist as kinesthetic haptic devices that can be categorized with respect to the energy source they use: pneumatics [1], hydraulics [2], electrodynamics [3], electromagnetics [4]; their control structure: open-loop impedance [5], closed-loop impedance [6], closed-loop admittance [7]; the human body part they target: hand [8], arm [9] and the entire body [10]; being grounded or not: wearables [11,12], ground fixed [13,14]; mechanism type: serial [13], parallel [9], hybrid [3]; being biomechanical (using human bones/ joints) [15] or standalone [12]. HIPHAD v1.0 is a kinesthetic haptic device that uses electrical energy to run motors, has open-loop impedance type control structure, which targets the hand motion of the human while the human is seated on a chair working on a desk.

The mechanism of HIPHAD v1.0 is a hybrid combination of a spatial 3 degree-of-freedom (DoF) translational parallel mechanism and a 3 DoF serial spherical orientation mechanism [16]. The parallel mechanism is based on the R-CUBE design [17].

In a previous work on the dynamic analysis of the HIPHAD v1.0 haptic device, the R-CUBE mechanism orientation was changed from its original orientation to a new orientation in which the gravitational effects are equally shared among the actuators. The dynamic equation of motion for the R-CUBE mechanism was developed analytically and verified via simulation studies.

In this paper, the analytical equations of motions are experimentally tested on a manufactured R-CUBE mechanism prototype. However, the R-CUBE mechanism is re-oriented for better operator ergonomics so that the operator can work seated. The next section provides brief introduction of the HIPHAD device kinematics in its new orientation. The quasi-static force analysis is reformulated with respect to the new orientation. Finally, experimental set-up to validate the quasi-static force analysis is described and the test results are presented to verify the gravity compensation calculation and to characterize the device performance.

2. Kinematics of HIPHAD

In the operation procedure of the HIPHAD device, motion demands of the user are based the wrist point position with respect to the base frame by utilizing the real-time measurements from the position sensors in direct kinematics equations. S parameter in Fig. 1 is the distance from the origin to the related actuation axis along related base frame axis and it is constant for all

axes. This parameter defines the workspace location with respect to the origin, O. Homing position of the mechanism is defined to be in the middle of its workspace.

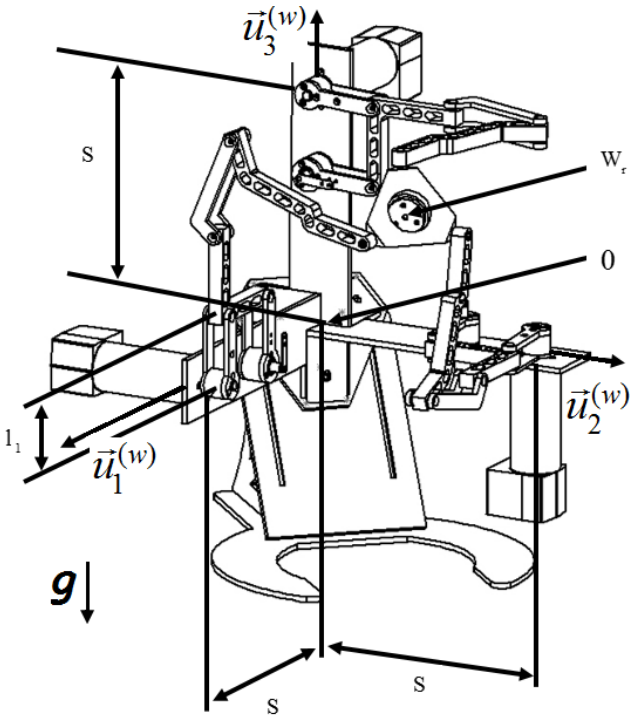

Fig. 1. A sketch of the translational parallel mechanism with its main parameters

Translational parallel mechanism of HIPHAD is an R-Cube mechanism, which has decoupled motion along base frame axes shown in Fig. 1 as $\vec{u}_i^{(w)}; i = 1,2,3$. Hence, motion along any base frame axis is generated by the actuator that has its rotation axis located on the respective base frame axis. In Equation (1), calculation of the position vector of the wrist point $\overrightarrow{OW_r}$ with respect to the base frame, $\mathcal{F} = \mathcal{F}\{0; \vec{u}_1^{(w)}, \vec{u}_2^{(w)}, \vec{u}_3^{(w)}\}$, is described.

$$\overrightarrow{W_r} = \sum_{i=1}^{3} W_{ri}\vec{u}_i^{(w)} \qquad W_{ri} = S + l_1 \cdot \sin(\theta_{i1}) \qquad (1)$$

The initial position of actuators that define the initial position of the wrist point are represented with a solid red line arrow and the angle limits are given in the Fig. 2.

Inverse kinematics of HIPHAD is provided for the whole kinematic chain including the calculation of passive joint positions on three legs. The actuated and passive joint angles in the kinematic chain of the leg i are given by θ_{i1}, θ_{i2}, θ_{i3} and θ_{i4}. These joint angles are provided in Fig. 2 and Fig. 3.

The mechanical structure of HIPHAD constrains the first link rotation to ±68° [16], and therefore, the solution for θ_{i1} is unique as formulated with σ equal to 1 in Equation (3).

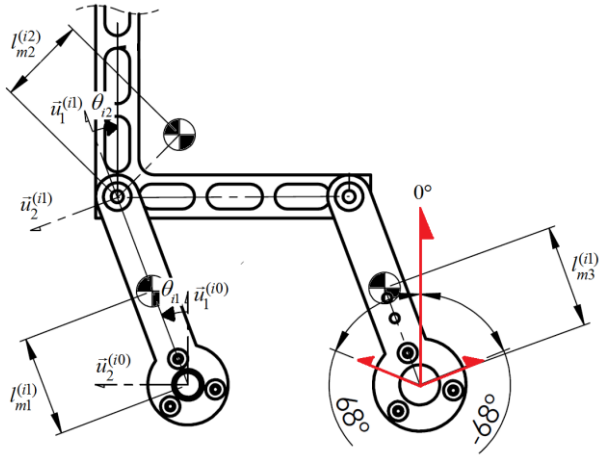

Fig. 2. Active and passive joint angles with mass center locations of parallelogram i

$$\sin(\theta_{i1}) = \frac{W_{ri} - S}{l_1} \qquad (2)$$

$$\cos(\theta_{i1}) = \sigma\sqrt{1 - \sin^2(\theta_{i1})} \qquad (3)$$

The solution for θ_{i1} using Equation (2) and (3) is given by

$$\theta_{i1} = \operatorname{atan2}(\sin(\theta_{i1}); \cos(\theta_{i1})) \qquad (4)$$

The second joint angle can be calculated by using the information of θ_{i1} as $\theta_{i2} = -\theta_{i1}$. The other joint angles are defined relative to the previous links as indicated in Fig. 3 and are calculated as these angles are calculated as

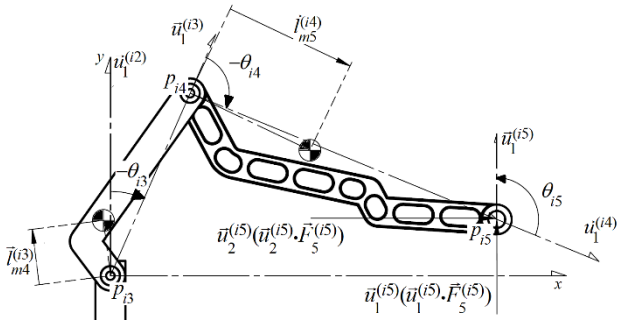

Fig. 3. Passive joint angles, mass center locations and

frame unit vector of limb i.

$$\theta_{i4} = \operatorname{atan}2\left(-\sqrt{1-\left(\frac{x_i^2+y_i^2-l_4^2-l_5^2}{2l_4l_5}\right)^2}\,;\frac{x_i^2+y_i^2-l_4^2-l_5^2}{2l_4l_5}\right) \quad (5)$$

$$\theta_{i3} = \operatorname{atan}2\left(-\sqrt{1-\left(\frac{x_i(l_4l_5\cos(\theta_{i4}))+y_i(l_5\sin(\theta_{i4}))}{x_i^2+y_i^2}\right)^2}\,;\frac{x_i(l_4l_5\cos(\theta_{i4}))+y_i(l_5\sin(\theta_{i4}))}{x_i^2+y_i^2}\right) \quad (6)$$

In Equations (5) and (6), x_i and y_i denotes the joint position P_{i5} with respect to P_{i3} with respect to the plane defined by $x-y$ axes in Fig. 3. Here the x_i and y_i location of P_{i5} is determined by the location of the other two limbs of HIPHAD. It is possible to identify the location of P_{i5} with the notation in Fig. 4, where Cp platform dimension constant, Cx is a constant shift and Cy is the location of P_{i3} along the y direction by solving the following expressions

$$\begin{aligned} x_1 &= W_{r2} - C_x - C_p \\ y_1 &= W_{r3} - {C_y}^1 - C_p \\ x_2 &= W_{r3} - C_x - C_p \\ y_2 &= W_{r1} - {C_y}^2 - C_p \\ x_3 &= W_{r1} - C_x - C_p \\ y_3 &= W_{r2} - {C_y}^3 - C_p \end{aligned} \quad (7)$$

$${C_y}^i = \vec{u}_1^{(i0)} \cdot \left(l_1\vec{u}_1^{(i1)} + l_2\vec{u}_1^{(i2)}\right)$$

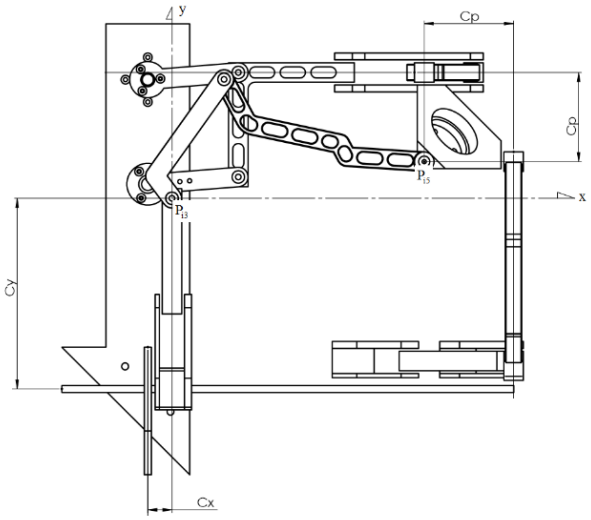

Fig. 4. Top view of HIPHAD

The positions of mass centers and edge points of the links are required for quasi-static equilibrium analysis and this needs the calculation of orientation and translation of each link's frame. The transformation matrices between the frames are given in Equation set (8) and these matrices will be used in dynamic calculation in next section. The frames are indicated in Fig. 5 and i is an index for one of the three limbs of HIPHAD.

In order to have a common matrix notations, in this work, for the same parameter u, if it is a column matrix, it is shown as $\bar{u}$; if it is a non-colum matrix, it is shown as $\hat{u}$; if it is a skew-symmetric matrix, it is shown as $\tilde{u}$.

$$\begin{aligned} \hat{C}^{(i0,i1)} &= e^{\tilde{u}_3\theta_{i1}} \\ \hat{C}^{(i1,i2)} &= e^{-\tilde{u}_3\theta_{i1}}e^{-\tilde{u}_1\pi/2} \\ \hat{C}^{(i2,i3)} &= e^{-\tilde{u}_3\theta_{i3}} \\ \hat{C}^{(i3,i4)} &= e^{-\tilde{u}_3\theta_{i4}} \\ \hat{C}^{(i4,i5)} &= e^{\tilde{u}_3\theta_{i5}} \end{aligned} \quad (8)$$

Using the above transformation matrices, overall transformation matrix for limb i can be calculated as

$$\begin{aligned} \hat{C}^{(i0,i5)} &= \hat{C}^{(i0,i1)}\hat{C}^{(i1,i2)}\hat{C}^{(i2,i3)}\hat{C}^{(i3,i4)}\hat{C}^{(i4,i5)} \\ \hat{C}^{(i0,i5)} &= e^{-\tilde{u}_1\pi/2}e^{-\tilde{u}_3(\theta_{i3}+\theta_{i4}-\theta_{i5})} \end{aligned} \quad (9)$$

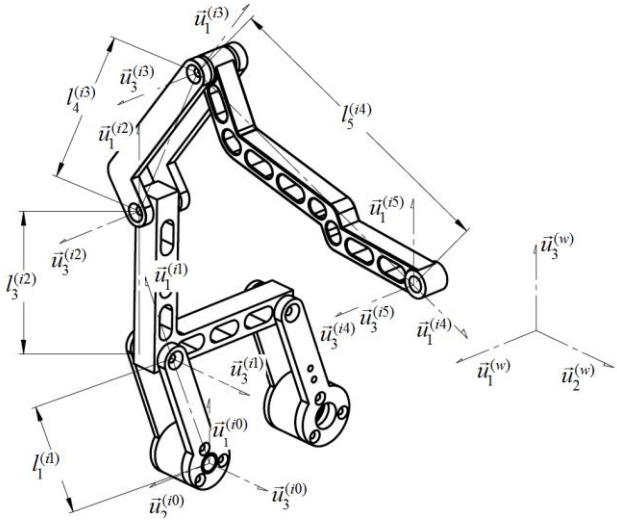

Fig. 5. A schematic representation with link frames of one of the limbs of HIPHAD

It should be noted that θ_{i5} basically equal to the summation of θ_{i4} and θ_{i3}. Therefore, rotation matrix for the last frame can be simplified as

$$\hat{C}^{(i0,i5)} = e^{-\tilde{u}_1\pi/2} \quad (10)$$

The orientations of each limb are calculated with respect to the frames of their first link. The corresponding rotations in world frame formulations are

expressed as

$$\begin{aligned}\hat{C}^{(w,10)} &= e^{-\tilde{u}_3\pi/2}e^{-\tilde{u}_2\pi/2}\\ \hat{C}^{(w,20)} &= \hat{I}\\ \hat{C}^{(w,30)} &= e^{\tilde{u}_2\pi/2}e^{\tilde{u}_3\pi/2}\end{aligned} \quad (11)$$

3. Quasi-Static Equilibrium Analysis of HIPHAD

HIPHAD is a kinesthetic haptic device which makes the user to feel forces at the handle of the device. This force is generated by torque input to the actuators of the haptic interface. In order to generate a desired force at the end effector, an analytic relationship must be established between the actuator torque and end effector force by making use of quasi-static analysis.

Newton-Euler method is used for the quasi-static equilibrium analysis. The reason for choosing this method is due to the fact that resultant calculated forces includes the information of reaction forces and torques in addition to the actuation force and torques for every joint. Quasi-static equilibrium analysis should start with the calculation of the torques and forces of the 4th and 5th links caused by the gravitational acceleration. With that, $\vec{F}_5^{(i5)}$ force at the P_{i5} point on $\vec{u}_1^{(i5)}$- $\vec{u}_2^{(i5)}$ plane can be determined and recursive calculations can initiate from p_{i5} point to the 0th frame. This force can be calculated by using

$$\begin{aligned}\vec{M}_2^{(i2)} &= \left(\vec{l}_4^{(i3)} + \vec{l}_{m5}^{(i4)}\right)\times\vec{g}^{(w)}m_5\\ &\quad + \left(\vec{l}_{m4}^{(i3)}\right)\times\vec{g}^{(w)}m_4\\ &\quad + \left(\vec{l}_4^{(i3)} + \vec{l}_5^{(i4)}\right)\\ &\quad \times\vec{F}_5^{(i5)} = 0\\ \vec{M}_3^{(i3)} &= \left(\vec{l}_{m5}^{(i3)}\right)\times\vec{g}^{(w)}m_5\\ &\quad + \left(\vec{l}_5^{(i4)}\right)\times\vec{F}_5^{(i5)}\\ &\quad = 0\end{aligned} \quad (12)$$

where $\vec{M}_2^{(i2)}$ and $\vec{M}_3^{(i3)}$ are the moments at the corresponding frames, $\vec{g}$ is the gravitational acceleration, $\vec{l}_4^{(i3)}$ and $\vec{l}_5^{(i4)}$ are the link lengths in vector form, $\vec{l}_{m4}^{(i3)}$ and $\vec{l}_{m5}^{(i4)}$ are the mass center position vectors and m_4 and m_5 are the masses of 4th and 5th links, respectively.

It should be noted that, since $\vec{F}_5^{(i5)}$ is calculated in $\vec{u}_1^{(i5)}$-$\vec{u}_2^{(i5)}$ plane, the $\vec{u}_3^{(i5)}$ component of $\vec{F}_5^{(i5)}$ will always be 0. The other components of $\vec{F}_5^{(i5)}$ are compensated by the actuators that are connected the other limbs. In this concept, although the forces within the ith serial chain (limb) are summed up recursively, the components of $\vec{F}_5^{(i5)}$ force should be subtracted from the ith limb and added to the corresponding neighboring limbs along with the external forces generated by the human acting on P_{i5}.

The total force equilibrium at the 4th frame of each limb system including the externally applied force to the platform $\bar{F}_{5ext}^{(w)}$ can be written in the matrix form as

$$\begin{aligned}\bar{F}_{34}^{(14)} &= \bar{u}_3^{(14)}\left(\bar{u}_3^{(14)}\right)^T\hat{C}^{(14,w)}\bar{F}_{5ext}^{(w)}\\ &\quad + \hat{C}^{(14,w)}\bar{g}^{(w)}m_5\\ &\quad - \hat{C}^{(14,15)}\bar{F}_5^{(15)}\\ &\quad + \bar{u}_3^{(14)}\left(\left(\bar{u}_1^{(25)}\right)^T\cdot\bar{F}_5^{(25)}\right)\\ \bar{F}_{34}^{(24)} &= \bar{u}_3^{(24)}\left(\bar{u}_3^{(24)}\right)^T\hat{C}^{(24,w)}\bar{F}_{5ext}^{(w)}\\ &\quad + \hat{C}^{(24,w)}\bar{g}^{(w)}m_5\\ &\quad - \hat{C}^{(24,25)}\bar{F}_5^{(25)}\\ &\quad + \bar{u}_3^{(24)}\left(\left(\bar{u}_2^{(15)}\right)^T\cdot\bar{F}_5^{(15)}\right)\\ \bar{F}_{34}^{(34)} &= \bar{u}_3^{(34)}\left(\bar{u}_3^{(34)}\right)^T\hat{C}^{(34,w)}\bar{F}_{5ext}^{(w)}\\ &\quad + \hat{C}^{(34,w)}\bar{g}^{(w)}m_5\\ &\quad + \bar{u}_3^{(34)}\left(\left(\bar{u}_2^{(25)}\right)^T\cdot\bar{F}_5^{(25)}\right.\\ &\quad \left.+ \left(\bar{u}_1^{(15)}\right)^T\cdot\bar{F}_5^{(15)}\right)\end{aligned} \quad (13)$$

It should be noted that $\bar{F}_5^{(35)}$ does not appear in the equation for $\bar{F}_{34}^{(34)}$. The reason for this is that since the gravitational force acts along the $-\vec{u}_3^{(35)}$-axis, this force does not generate any moment that cause a motion of the 4th and 5th links.

General representation can be used for remaining recursive force calculations as

$$\begin{aligned}\bar{F}_{23}^{(i3)} &= \hat{C}^{(i3,i4)}\bar{F}_{34}^{(i4)} + \hat{C}^{(i3,w)}\bar{g}^{(w)}m_4\\ \bar{F}_{12}^{(i2)} &= \hat{C}^{(i2,i3)}\bar{F}_{23}^{(i3)} + \hat{C}^{(i2,w)}\bar{g}^{(w)}m_2\end{aligned} \quad (14)$$

where m_4 and m_2 are the masses of the links, and $\bar{F}_{23}^{(i3)}$ and $\bar{F}_{12}^{(i2)}$ are the resultant forces on the 2nd and 1st frames, respectively.

It should be noted that $\bar{F}_{01}^{(i1)}$ force is not calculated since this force acts on the actuator shaft which is carried by the bearing and does not result in any motion of any movable parts.

Finally, by making use of above equations, resultant torque on the actuators can be calculated as

$$\begin{aligned}&\bar{T}_1^{(10)}\\ &= \mathrm{smm}\left(l_1\hat{C}^{(10,11)}\bar{u}_1^{(11)}\right)\hat{C}^{(10,12)}\bar{F}_{12}^{(12)}\\ &+ \mathrm{smm}\left(\bar{l}_{m1}^{(10)}\right)\hat{C}^{(10,w)}\bar{g}^{(w)}m_1\\ &+ \mathrm{smm}\left(\bar{l}_{m3}^{(10)}\right)\hat{C}^{(10,w)}\bar{g}^{(w)}m_3\end{aligned} \quad (15)$$

$$\begin{aligned}
&\bar{T}_2^{(20)} \\
&= \mathrm{smm}\left(l_1 \hat{C}^{(20,21)} \bar{u}_1^{(21)}\right) \hat{C}^{(20,22)} \bar{F}_{12}^{(22)} \\
&+ \mathrm{smm}\left(\bar{l}_{m1}^{(20)}\right) \hat{C}^{(20,w)} \bar{g}^{(w)} m_1 \\
&+ \mathrm{smm}\left(\bar{l}_{m3}^{(20)}\right) \hat{C}^{(20,w)} \bar{g}^{(w)} m_3 \\
&\bar{T}_3^{(30)} \\
&= \mathrm{smm}\left(l_1 \hat{C}^{(30,31)} \bar{u}_1^{(31)}\right) \hat{C}^{(30,32)} \bar{F}_{12}^{(32)} \\
&+ \mathrm{smm}\left(\bar{l}_{m1}^{(30)}\right) \hat{C}^{(30,w)} \bar{g}^{(w)} m_1 \\
&+ \mathrm{smm}\left(\bar{l}_{m3}^{(30)}\right) \hat{C}^{(30,w)} \bar{g}^{(w)} m_3 \\
&+ \mathrm{smm}\left(l_1 \hat{C}^{(30,31)} \bar{u}_1^{(31)}\right) \hat{C}^{(30,w)} \bar{g}^{(w)} m_{\mathrm{platform}}
\end{aligned}$$

where $\overrightarrow{T_1}$, $\overrightarrow{T_2}$ and $\overrightarrow{T_3}$ are the torques on the related actuators; m_1 and m_3 are the masses of the link 1 and link 3; l_1 is the length of link 1; $\vec{l}_{m1}^{(i0)}$ and $\vec{l}_{m3}^{(i0)}$ are the mass center position vectors that are defined with respect to the 0^{th} frame of the i^{th} limb that originate from their respective rotation centers. In this equation set, smm(·) operator is used to transform column matrices to skew-symmetric (cross-product) matrices.

It should be noted that only 3rd serial chain (limb) carries the weight of platform which is $\bar{g}^{(w)} m_{\mathrm{platform}}$. Here, m_{platform} is the mass of the mass of the mobile platform.

4. Experimental Verification

Initially, the analysis results are verified through simulations. Verification of these calculations are executed in MATLAB Simulink using first generation of SimMechanics module. The CAD model of HIPHAD is translated to the Simulink environment. Calculations of the quasi-static equilibrium equations and SimMechanics model simulation are executed simultaneously and resulting forces obtained from the simulation of HIPHAD and mathematical model is compared. In simulation tests, HIPHAD is positioned in several points step by step and through the workspace of the device. The difference between the torques that are calculated by using the equations and SimMechanics model came out to be in the range of 10^{-8} Nm for static tests in which the maximum torque calculated was around 0.3 N·m. The difference can be considered in an acceptable range for numerical errors. In order to verify the analysis results by experimentation, the first work is carried out to match the real system working conditions to the ideal model as much as possible. The first consideration is about the assumption that the gravitational acceleration acts along the $-\vec{u}_3^{(w)}$ axis; however, due to the deformation in the base of HIPHAD this assumption is not valid. Therefore, basement of HIPHAD has to be corrected by orienting it on the ground so that its $\vec{u}_1^{(w)}$, $\vec{u}_2^{(w)}$ and $\vec{u}_3^{(w)}$ axes are aligned with the world frame coordinates.

The second and final work before running the calibration routines for the motion and force exertion of the device is carried out for matching the inertial properties of the device with the model. Although the mathematical and SimMechanics models match, the resultant dynamic forces of these two cannot be compared to the results of the experiments since the inertia of components of the real device might differ due to some non-idealities such as manufacturing faults, bearing and fasteners that are not considered in the model. The source of this possible error is compensated by weighing every component of the links, which are screws and links, within 0.02 g tolerance scales and the obtained values are added to mathematical model and also the mass center positions are recalculated.

Next, the experimental setup was established to conduct tests of the device, which is denoted with 1 in Fig. 6. In each limb, YUMO E6B2-CWZ3E incremental encoders, which are denoted with 3 in Fig. 6, are used on one of the legs of the parallelograms to measure the rotation of the first link and on the other leg the Maxon EC 45 brushless DC actuators, which are denoted with 2 in Fig. 6, are used provide moment to the respective limb. It should be noted that no reduction system is used and this characterizes the system as a direct-drive system. Maxon 4-Q-EC Amplifier 70/10 drivers, which are denoted with 4 in Fig. 6, are used to drive the actuators. The information exchange between the components and the control computer is established via Humusoft MF624 data acquisition (DAQ) card, which is denoted with 5 in Fig. 6, by using MATLAB 2014a Simulink in external real-time windows target mode. Shielded cables are used to minimize the noise effects on analog signals between the DAQ and drivers. The sampling time is selected as 1 ms.

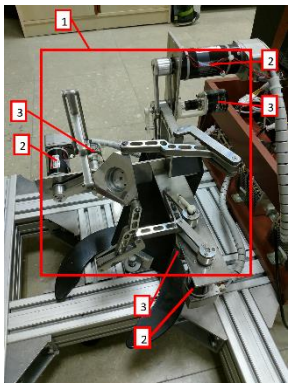

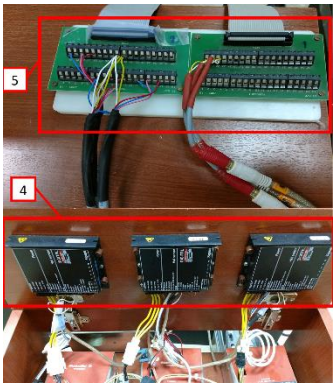

Fig. 6. Experimental setup components

After the necessary connections are made, the offset values for drivers are set to sustain the positioning of the actuator shafts when there are no loads attached to them. This offset value sets the amount of current supplied to actuator when the controller signal is zero. Torques comments to be supplied to the actuators in experiments are received in VDC. Therefore, they are multiplied by the torque constant that is given in datasheet as 45.5 mN·m/A. However, the driving signal send to the drivers is in VDC so a mapping is required to determine generated current per given VDC. Since the drivers can receive ±10VDC driving signals and Humusoft MF624 can send ±10VDC driving signal, this corresponds to 1 to 1 mapping and 45.5 mN·m/VDC torque constant can be used instead. This mapping is confirmed by monitoring the output current from the driver for a given VDC signal by using 'monitor' port on the driver. Also, a certain amount of torque is exerted to the actuator externally and the amount of current to withhold this external torque is measured, which matched with the datasheet value of 45.5 mN·m/A. The exchange of the information among the components of the experimental setup is represented in Fig.7.

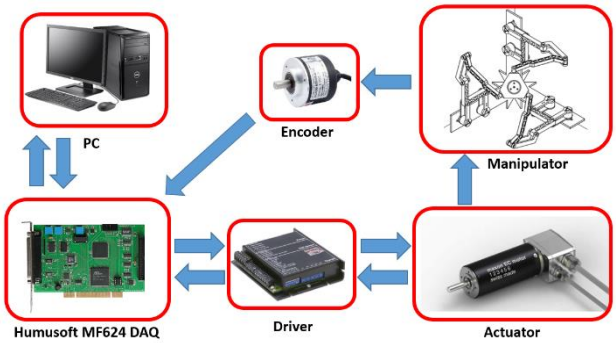

Fig. 7. Information exchange among the experimental setup components

Due to its mechanical limitations, parallelograms of each limb can move a total of 136° about their axis of motion and this full range is divided into half which are negative and positive partitions. This data is verified by tests in which the zero position of parallelograms is the middle points of the full range as it is illustrated in Fig. 2. A detailed motion calibration procedure of this device when potentiometers as position sensors was used is provided in [18].

The control algorithm of HIPHAD that was used in the tests has phases that are run one after another within a procedure. The first step of this procedure is homing and this phase of the algorithm works every time the device is initiated. This sub-controller provides enough amount of torque to settle the mechanism to its most extended and the most folded positions and record the angular positions of the actuators. After acquiring the positions of the actuator at the workspace limits, zero (initial) position of the mechanism is calculated. Then, HIPHAD's moving platform is moved to this zero position using a PID controller. This PID controller closes the feedback control loop by using the joint sensors (encoders). Once this sub-controller finishes its routine, HIPHAD is ready for the tests.

In the experiments, initially, torques generated by the actuators are measured for maintaining static conditions at every integer angular position which results in discontinuous measurements. Secondly, full range of mechanism is scanned by moving the device in each axis by a 0.25 °/s speed and actuator torques are measured. Dynamic motion effects generated in slow operation are calculated to be in the range of ± 6.10^{-9} N·m in the simulation tests and thus, they can be neglected. As a matter of fact, experiment results showed that there is a small difference between continuous and discontinuous motion experiments. Although the values of the outputs were not exactly the same for the recorded positions, the behavior of both errors resembled each other.

The amounts of torques supplied to each actuator during the motion along their respective axis by a 0.25 °/s speed are shown Fig. 8. It should be noted that during the motion along one axis the others are locked at their zero positions in order to identify the calculation errors of the torques generated by the specific axis motors. A PID controller is used to regulate the motion at the required speed to move from the folded positions to extended positions (in between the workspace boundaries). The actuator that provides motion along the $\vec{u}_3^{(w)}$ axis results in highest torque generation since it axis of action is aligned with the gravity axis. Nevertheless, the result for this axis reveals some anomalies. These are the sharp corners which normally should not exist and this can be seen when the devices reaches -34° and +22°

in $\vec{u}_3^{(w)}$ axis.

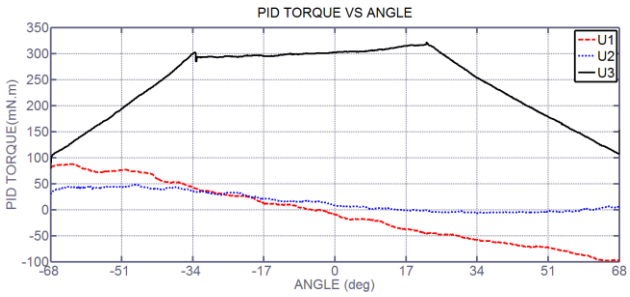

Fig. 8. The measured torques as applied by PID controller

The error between the measured and the calculated torques are calculated and plotted in Fig. 9. In this figure, it can be clearly observed that the peak errors for the calculations in the $\vec{u}_3^{(w)}$ axis actuator occur at -34° and +22° angular positions.

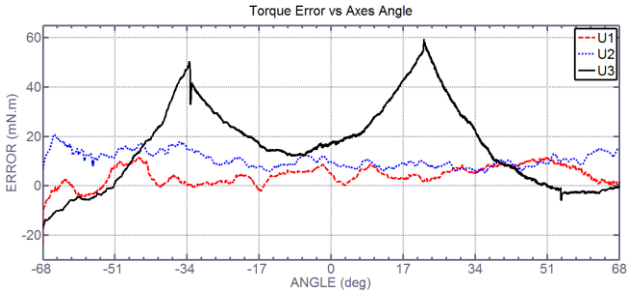

Fig. 9. Calculated error for torques supplied by each axis actuator. (T_{error}=$T_{calculated}$-T_{PID})

When the calculations and measurements made for the $\vec{u}_1^{(w)}$ axis actuator is individually examined, measured torques and calculated ones almost perfectly overlap with each other as shown in Fig. 10. The maximum error is around 10mN·m. Throughout the whole scanned range, the maximum nominal error is around +5 mN·m. The error distribution for the scanned range varies as a result of the applied torque range.

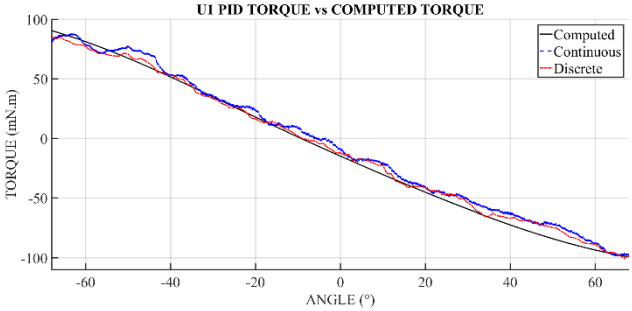

Fig. 10. Calculated Torque vs measured torque for $\vec{u}_1^{(w)}$ axis motion.

The measured torques in $\vec{u}_2^{(w)}$ axis shows a constant offset of +10mN·m from the calculated torques yet it can follow the calculated torque values as shown in Fig. 11.

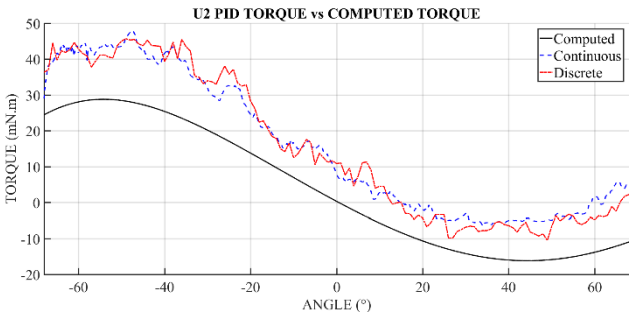

Fig. 11. Calculated Torque vs measured torque for $\vec{u}_2^{(w)}$ axis motion

Fig. 12 shows that the error in the measurements versus the calculated torques for the $\vec{u}_3^{(w)}$ axis actuator has a different characteristic compared to the errors calculated for the previous axis actuator torques. In the previous ones, the errors are almost constant however, the error revealed for axis $\vec{u}_3^{(w)}$ seems to heavily depend on the angular position of the actuator on $\vec{u}_3$.

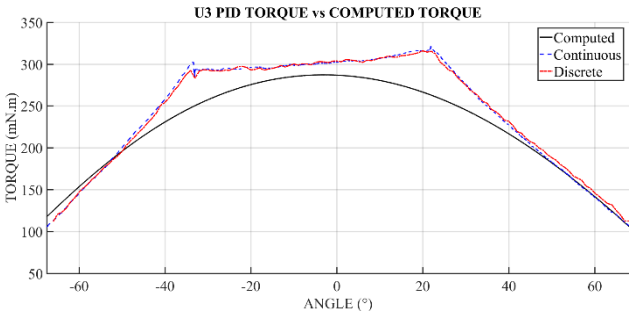

Fig. 12. Calculated Torque vs measured torque for $\vec{u}_3^{(w)}$ axis motion

The actuator providing the motion along the $\vec{u}_3^{(w)}$ axis carries most of the weight of the manipulator and thus, this actuator generates the highest overall torques. The experiments revealed that it has the highest errors at the angles -34° and +22° with 50 mN·m and 60 mN·m torque errors, respectively. A 'tick' sound is heard at these angles. Maxon EC 45 actuators are brushless three-phase actuators and the 'tick' sound is an indication of the phase transitions. The nonlinearity in generated torques during this mechanical phase transitions becomes more noticeable at higher torque values such as the torques generated by this actuator. This is the main

reason that there are higher errors in the vicinity of these phase transitions.

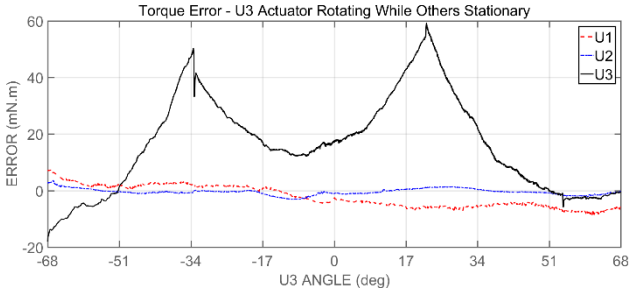

Fig. 13. Computed error data while there is a motion along $\vec{u}_3^{(w)}$ with 0.25 °/s and there is no motion along the other axes

A final test is carried out to understand the errors calculated for the $\vec{u}_1^{(w)}$ and $\vec{u}_2^{(w)}$ axes actuators. A 0.25 °/s speed slow motion provided along the $\vec{u}_3^{(w)}$ axis while keeping the positions along the other axes are maintained at their zero position by control. During this motion, the torques supplied to the $\vec{u}_1^{(w)}$ and $\vec{u}_2^{(w)}$ axes actuators are acquired. Then, the torque errors of these two axes actuators are calculated. In the full range of motion along $\vec{u}_3^{(w)}$ axis, the torque errors of the other two axes range between ±10mN·m as provided in Fig. 13. The cause of the errors of $\vec{u}_1^{(w)}$ and $\vec{u}_2^{(w)}$ is that the mechanism's frame is not exactly orthogonal and matched with the world frame.

6. Conclusions

In this work quasi-static equilibrium analysis of a haptic device is presented. The analysis results are first verified through a simulation model which is generated by using Matlab SimMechanics model. Then, the analysis results are experimentally tested.

The experiments revealed that the equations derived as a result of the analysis matches the experimental results in a larger extend for the actuators that provide motion along $\vec{u}_1^{(w)}$ and $\vec{u}_2^{(w)}$ axes. The errors that are calculated between the computed torques and measured torques can be considered as related with the imperfections of the mechanism frame's orthogonality and alignment with the world frame. These errors can be minimized by calculating the deviation of the mechanism frame from the ideal model.

The phase transition locations of the actuator that provides motion along the $\vec{u}_3^{(w)}$ are much more noticeable than the other two actuators due to the increased torque demands. The errors in torque calculations become larger in the vicinity of these phase transitions.

During the experimentation, it was also observed that actuators heat up in time causing a reduction of performance over time. The main reason of the heating of the actuators is due to the gravitational load.

The characterization of the device's static operation is completed by the experimental tests. One of the main observations is that for a better matching between the calculations and the actual system performance, passive balancing with respect to gravity can be implemented. This will reduce the work load of the actuators and thus, decrease the heating problem and amplification of the phase transition effects.

As future work, the analysis presented in this paper can be extended to account for the imperfections of the device such as the frame deviations and actuator's phase transitions. Also, a work on the dynamic analysis and verification of this dynamic analysis will be carried out.

Acknowledgements

This work is partially supported by The Scientific and Technological Research Council of Turkey via grant number 115E726.

References

[1]. M.Takaiwa & T.Noritsugu, Application of Pneumatic Parallel Manipulator as Haptic Human Interface, IEEE/ASME International Conference on Advanced Intelligent Mechatronics, Atlanta, GA, USA, September 19-23, 1999.

[2]. E.L.Faulring, J.E.Colgate and M.A.Peshkin, A high performance 6-DOF haptic Cobot, Robotics and Automation, Proceedings. ICRA '04. 2004 IEEE International Conference on, pp. 1980-1985 Vol.2., 2004

[3]. Web, http://www.forcedimension.com/products/sigma-7/overview (2017)

[4]. M.Benali-Khoudja, M.Hafez & A.Kheddar, VITAL: An electromagnetic integrated tactile display, Displays, vol. 28, is. 3, pages 133–144, 2007.

[5]. Kang Wen, D. Necsulescu and G. Basic, Development system for a haptic interface based on impedance/admittance control, Proceedings. Second International Conference on Creating, Connecting and Collaborating through Computing, pp. 147-151, 2004.

[6]. C.R.Carignan, & K.R.Cleary, Closed-loop force control for haptic simulation of virtual environments, 2000.

[7]. A.Peer & M.Buss, A New Admittance-Type Haptic Interface for Bimanual Manipulations, IEEE/ASME Transactions On Mechatronics vol. 13, is. 4, pages 416–428, 2008.
[8]. Web, http://www.dextarobotics.com (2017)
[9]. C.Carignan, J. Tang & S. Roderick, Development of an Exoskeleton Haptic Interface for Virtual Task Training, The 2009 IEEE/RSJ International Conference on Intelligent Robots and Systems, St. Louis, USA, October 11-15, 2009.
[10]. Web, http://axonvr.com/#virtual-reality-you-can-feel (2017)
[11]. J.Sone, R.Inoue, K.Yamada, T.Nagae, K.Fujita & M. Sato, Development of a Wearable Exoskeleton Haptic Interface Device, Journal of Computing and Information Science in Engineering, vol. 8, is. 4, pages 041009-1:12, 2008.
[12]. Schiele, André, and Gerd Hirzinger. "A new generation of ergonomic exoskeletons-the high-performance x-arm-2 for space robotics telepresence." Intelligent Robots and Systems (IROS), 2011 IEEE/RSJ International Conference on. IEEE, 2011.
[13]. P.Gallina & G.Rosati, Manipulability of a planar wire driven haptic device, Mechanism and Machine Theory, vol. 37, is. 2, pages 215-228, 2002.
[14]. J.W.Kim, D.H.Park, H.S.Kim & S.H.Han, Design of a Novel 3- DOF Parallel-type Haptic Device with Redundant Actuation, International Conference on Control, Automation and Systems, Seoul, Korea, Oct. 17-20, 2007.
[15]. Yang, Guilin, et al. "A haptic device wearable on a human arm." Robotics, Automation and Mechatronics, 2004 IEEE Conference on. Vol. 1. IEEE, 2004.
[16]. T.Bilgincan, E.Gezgin, and M. I. C.Dede, "Integration of the Hybrid-Structure Haptic Interface HIPHAD v1.0,": Proceedings of the International Symposium of Mechanism and Machine Theory, Izmir, Turkey, pp. 267-284, October 5-8, 2010.
[17]. Li, W., Gao, F., and Zhang, J.: R-CUBE, a Decoupled Parallel Manipulator only with Revolute Joints, Mech. Mach. Theory, 40, 467-473, 2005.
[18]. M.İ.C. Dede, B.Taner, T.Bilgincan, and M. Ceccarelli "Kinematic Analysis Validation and Calibration of a Haptic Interface," Advances on Theory and Practice of Robots and Manipulators Mechanisms and Machine Science, Marco Ceccarelli and Victor A. Glazunov (Eds.), Volume 22, pp 375-381 Springer, Dordrecht, The Netherlands, 2014 (ISBN: 978-3-319-07057-5).

EasyLap-New Robotic System for Single and Multiple Access Laparoscopy Using almost only Traditional Laparoscopic Instrumentation

Gionata FRAGOMENI[1], Gianluca GATTI[2], Pasquale F. GRECO[2], Paola NUDO[3], Michele PERRELLI[2], Basilio SINOPOLI[3], Antonia RIZZUTO[1] and Guido DANIELI[3*]
[3*]Calabrian High tech S.r.l.
Via Ponte Bucci Cubo 45C – 87036 Rende (CS)-Italy
E-mail: guido.danieli@unical.it
[1] Magna Græcia University - 88100 Catanzaro (CZ)-Italy
[2] DIMEG – Calabria University – 87036 Rende (CS)-Italy

Abstract
A new robotic system for single and multiple access laparoscopy is presented, using almost only traditional laparoscopic instrumentation, including very small diameter instruments for babies, based on an evolution of previous research by this research group. Main idea behind this system is to make simple its use, for instance instructing the optics to point always the tip of the instrument on which the surgeon is acting in a totally automatic way; a second important feature is the ability to guide also the motion of the instrument on which the surgeon is acting so that it corresponds to the joystick motion as seen from the monitor. All instruments are traditional, but for a special edition of SAL Twin Forceps, and a second instrument similar to the wrist of da Vinci but reusable and sterilizable since it uses only rods and gears for its motion.
Keywords: Robotized System for Traditional